# 層級焊點 HFCBGA 封裝模型之可靠度分析驗證

# Global-to-Local Modeling and Experiment Investigation of a HFCBGA Package Board-level Solder Joint Reliability

伍紹鈞<sup>1</sup> 陳精一<sup>2</sup>

Shao-Chiun Wu, Ching-I Chen

1空軍航空技術學院飛機工程系

2中華大學機械工程學系

<sup>1</sup> Aircraft Engineering

Air Force Institute of Technology

<sup>2</sup> Department of Mechanical Engineering

Chung Hua University

# 摘要

由於電子產品處理功能需求速度越來越快,驅使半導體封裝腳數的需求越來越高,使得傳統有限元素法的需求更加複雜及面對更大的挑戰。本文將探討 3-D 建模技巧方法,以研究層級焊點處於溫度循環下的可靠度分析並以等量全域模型作法使完整敘述錫點破壞的位置。而伴隨實驗數據的提供,使得高功率覆晶 HFCBGA (High performance Flip-Chip Ball Grid Array)封裝研究更具參考價值。最後,根據有限元素法的結果表示,所預測的錫球破裂位置與實驗結果相近。本研究 Global-to-Local 建模技術將提供一有效率的方法,來評估高腳數 HFCBGA 封裝之可靠度。關鍵字:有限元素法,高功率覆晶封裝,錫球接點可靠度,疲勞壽命

#### Abstract

Due to the high speed and high I/O count for semiconductor package requirements, thousands of soldered interconnections are indispensable, and this situation renders the traditional finite element method (FEM) analysis a formidable challenge. This paper presents a 3-D equivalent global model and local submodeling technique to investigate board-level solder joint reliability under temperature cyclic loading. The equivalent global model is capable of addressing cirtical solder failure locations. Individual local solder ball is then used to predict number of cycles to failure. A HFCBGA (High performance Flip-Chip Ball Grid Array) package case was studied with the provided experiment data. According to the FEM result, predicted solder ball life is close to the experiment data. Therefore, Global-to-Local modeling technique can be concluded to provide an efficient methodology for evaluating very high pin count HFCBGA (High performance Flip-Chip Ball Grid

Array) package reliability.

**Key Words:** Finite element method, HFCBGA package, solder joint reliability, fatigue life

# Introduction

The high speeds, high I/O counts, and high thermal dissipation required for semiconductor packages have resulted in flip chip design becoming the mainstream smaller-dimension package for ICs. Package failure depends on manifold characteristics of the infrastructure such as the geometric shape, the choice of the solder alloy, the material of the underfill, the broad construction, etc., which leads to serious reliability issues due to the thermal-mechanical problems under cyclic environments thermal loading Package-level reliability has been broadly studied including investigations underfill delamination and soldered bump fatigue failures. However, the major concern for board-level reliability is soldered ball fatigue failures. Generally, life the fatigue ofsoldered interconnections is estimated through finite element modeling [3-6] or through experimentation [7-9]. Solder reliability is still one of the most difficult problems for the electronics industry. Lee et al. [10] comprehensively summarized the existing solder joint fatigue models including stress-based, plastic strain-based, creep strain-based, energy-based and damagebased models.

On the other hand, various modeling techniques exist for predicting the fatigue life of a solder joint in a ball grid array (BGA) type [11]. These common modeling

techniques can be classified into 2-D plane strain model [12, 13], 3-D slice model [14, 15], 3-D full model [16, 17] and 3-D global model with a local submodel [18]. The 3-D full model uses quarter or octant symmetrical boundaries to reduce the computation time but modeling difficulty on the finite element mesh is due to the large scale difference between the solder ball and solder bump geometries. However, the global model employs a relatively coarse mesh for all components in the package except the critical solder ball and solder bump. The mesh generation aspect becomes time consuming because the fine mesh associated with the critical solder ball and solder bump must match the coarse mesh of the remaining components. Although more solders are allowed in the modeling, it is still not feasible if the package consists of a very large number of solders. No exiting modeling technique can predict the solder ball fatigue life without struggle, especially in when a huge amount of solder interconnections are involved. In this paper, a 3-D equivalent global model with local submodel technique developed capable of assessing solder ball reliability of very high pin count packaging form factor. This modeling technique combines the advantages of full modeling capability from a 3-D full model and local strain analysis from the 3-D global model with a local submodel. At the end of this paper, a HFCBGA (High performance Flip-Chip Ball Grid Array)

package was performed board-level reliability test to validate the prediction of the solder fatigue life.

# Packaging Geometry and Material Properties

Fig. 1 shows a high-performance FCBGA package, in which a heat spreader is attached to the topside of the package and supported by the stiffener ring. This packaging architecture enhances the thermal dissipation and also able to protect the brittle silicon die. A high power device is suitable for this form factor.

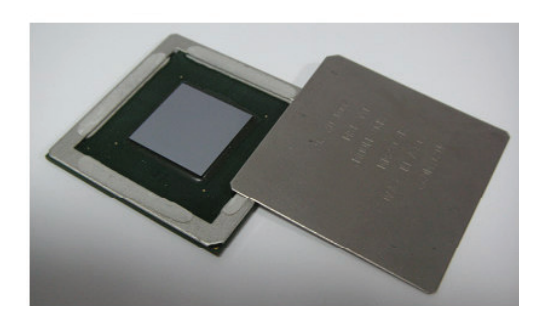


Fig. 1. High-performance FCBGA package.

Fig. shows cross-sectional a configuration and illustration HFCBGA package. The die size is 18 mm × 18 mm, the die thickness is 0.737 mm, the package body size is 42.5 mm× 42.5 mm, the sandwich substrate thickness is 1.2 mm including the built-up FR-4 layers (0.2 mm) on both sides of the BT core (0.8 mm), the heat spreader thickness is 0.5 mm, the printed circuit board (PCB) thickness is 1.6 mm, and the stiffener ring width is 4 mm. The width of the PCB is 63.75 mm, which is 1.5 times that of the substrate for FE simulation purposes.

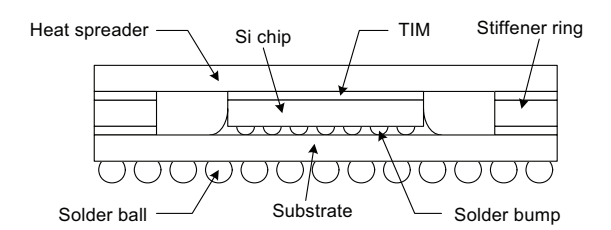


Fig. 2. Cross-sectional configuration and illustration of a HFCBGA package.

The elastic modulus (MPa) and yield stress (MPa) of 63Sn/37Pb eutectic solder was assumed to be temperature dependent given by [19]

$$E(T) = 75970 - 152T \tag{1}$$

$$\sigma(T) = 49.2 - 0.097T \tag{2}$$

where the T is temperature (K). The creep constitutive law for eutectic solder was referred from [20], which is given by

$$\dot{\varepsilon} = 10[\sinh(0.2\sigma)]^2 e^{-5401.2/T}$$
 (3)

where  $\dot{\varepsilon}$  is the equivalent creep strain rate,  $\sigma$  is the equivalent von Mises stress and temperature (K). The material properties used in the simulation are tabulated in Table I.

TABLE I
Material Properties for HFCBGA Package

	Tg	E (MPa)	CTE (ppm/℃)	Poisson ratio
Die		131000	2.6	0.28
TIM		0.35	232	0.38
		11557@-50℃	58.52@-50℃	
Adhesive		3933@50℃	58.52@0℃	0.35
		40.8@150℃	177.9@150℃	
Substrate		26000 (X, Y)	15 (X, Y)	0.11 (XY)
core material		11000 (Z)	52 (Z)	0.39 (XZ, YZ)
Underfill	70	7000/40	32/110	0.33
63Sn/37Pb solder		Eq. (1)	24.7	0.4
Solder mask		3450	30	0.35
Built-up		3500	60	0.22
Heat spreader/ring		117000	16.7	0.34
PCB		22000 (X, Y) 10000 (Z)	18 (X, Y) 70 (Z)	0.11 (XY) 0.28 (XZ, YZ)

# Global-to-Local Modeling

In order to apply the submodeling technique to solder ball, at least two models have to built, namely, a global model and a local submodel using commercial software ANSYS. The global model determines the overall package response. The local model is used to determine the solder ball reliability. The displacement solutions solved in the global model are interpolated into the local model along the cutting local boundaries.

### A. Global Modeling

In the global modeling, a quarter of the package was built because it behaves as a half of symmetry in two in-plane axes. Fig. 3 shows the global model where the package is mounted on a printed circuit board (PCB). This model does not include the detailed solder ball and solder bump geometries but uses equivalent layers. For the solder bump layer, the equivalent properties can be determined based upon the volumetric ratio.

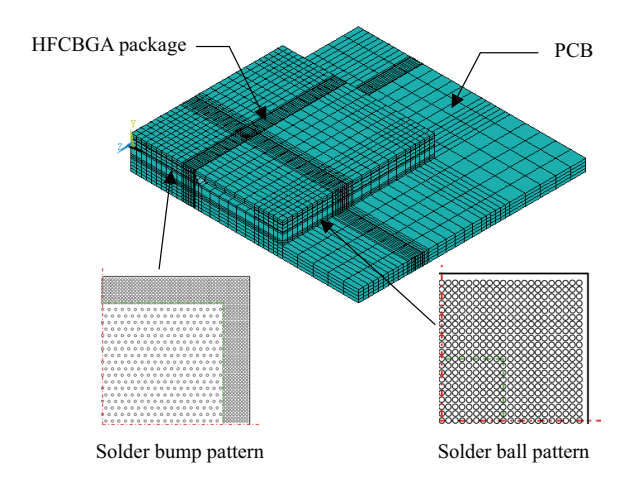


Fig. 3. 1/4 symmetric global model of HFCBGA package.

If V,  $V_{\mu}$  and  $V_{\mu}$  denote the total layer

volume, proportional underfill and solder volumes,  $n_u = V_u/V$ ,  $n_s = V_s/V$ , the mixtures expression rule for the elastic modulus, Poisson's ratio and CTE (Coefficient of thermal expansion) are expressed as [21]

$$E_{eq} = E_{u} n_{u} + E_{s} n_{s} \tag{4}$$

$$v_{eq} = v_u n_u + v_s n_s \tag{5}$$

$$\alpha_{eq} = \alpha_{u} n_{u} + \alpha_{s} n_{s} \tag{6}$$

where  $E_{eq}$ ,  $E_u$  and  $E_s$  are the equivalent, underfill and solder elastic moduli.  $v_{eq}$ ,  $v_u$  and  $v_s$  are the equivalent, underfill and solder Poisson's ratio.  $\alpha_{eq}$ ,  $\alpha_u$  and  $\alpha_s$  are the equivalent, underfill and solder CTE. For the solder ball layer, the terms relate to underfill refer (4) to (6) can be eliminated because the solder balls are mixed with air environment.

To get as close to the actual configuration as possible, the substrate is modeled as a sandwich structure where the middle layer is a rigid core and the upper and lower layers are build-up in global modeling. The detailed metal trace layout and density effect are not considered with the modeling difficulties. The mechanical properties of laminated composite plate, such as substrate and PCB, are critical for package overall response [22]. Basically, the organic substrate and PCB behave orthotropic. The elastic modulus, Poisson's ratio and CTE material properties in the axial directions can be easily determined using specific material experiments. However, the shear modulus is difficult to measure, especially in small dimensions. and cannot directly converted from other properties. Therefore, this research proposes approximation solution to approach the shear moduli based on the material mechanics. As long as the orthotropic material properties of the substrate core and PCB are given, the in-plane shear moduli can be approximated as

$$G_{xy} = \frac{E_x}{2(1 + v_{xy})} \tag{7}$$

and the out-of-plane shear modulus can be approximated as

$$G_{xz} = \frac{1}{2\left(\frac{1}{E_{y}} + \frac{V_{yz}}{E_{z}}\right)}, G_{yz} = \frac{1}{2\left(\frac{1}{E_{x}} + \frac{V_{xz}}{E_{z}}\right)}$$
(8)

where  $G_{xy}$ ,  $G_{xz}$  and  $G_{xy}$  are the shear moduli.  $E_x$ ,  $E_y$  and  $E_z$  are the elastic moduli.  $v_{xy}$ ,  $v_{xz}$  and  $v_{yz}$  are the Poisson's ratio.

# B. Local Modeling

The solder profile has great impact on the fatigue life prediction. An approximate mathematical model was used to predict the solder profiles in an array type interconnection [23]. This model is based on the assumption that the geometry of each solder may be represented by a rotary surface whose generating meridian is a circular arc. This leads to simple, close form expressions relating to the standoff height, solder volume, pads radii, package weight, reaction force, meridian curvature and surface tension of the solder. The geometric parameters predict the closedform single solder moduli are given as below:

h Standoff height;

- $r_1, r_2$  Radii of pads on the chip and substrate sides, respectively;
- $r_0, z_0$  Coordinates for the center curvature of the circular-arc meridian;
- rc Radii of the curvature of the circular-arc meridian;
- Vs Volume of the solder;

All geometric parameters are nondimensionalized using the standoff height h as a scale factor. Therefore, the dimensionless parameters can be determined as  $\rho_1 = r_1/h$ ,  $\rho_2 = r_2/h$ ,  $\rho_0 = r_0/h$ ,  $\varsigma_0 = z_0/h$ ,  $\bar{r}_c = r_c/h$ ,  $\bar{V} = V/h^3$ . The meridian's center of curvature ( $\rho_0$ ,  $\varsigma_0$ ) was obtained from the geometric parameters of the radius of curvature  $\bar{r}_c$  and the pads radii  $\rho_1$  and  $\rho_2$ .

$$\rho_0 = \frac{1}{2} \left[ \rho_1 + \rho_2 - \sqrt{\frac{4\bar{r}_c^2}{(\rho_1 - \rho_2)^2 + 1} - 1} \right]$$
 (9)

$$\varsigma_{0} = \frac{1}{2} \left[ 1 - (\rho_{1} - \rho_{2}) \sqrt{\frac{4\overline{r_{c}}^{2}}{(\rho_{1} - \rho_{2})^{2} + 1} - 1} \right]$$
 (10)

Because the solder cannot penetrate the pad materials, a minimum value of  $\bar{r}_c$  may be calculated from the geometry limitation. It can be expressed as

$$\bar{r}_{c \text{ (min)}} = \frac{1}{2} \left[ (\rho_1 - \rho_2)^2 + 1 \right] \tag{11}$$

The equation of circular-arc meridian may be written as

$$\rho(\varsigma) = \rho_0 + \sqrt{\overline{r}_c^2 - (\varsigma - \varsigma_0)^2} \tag{12}$$

Which was integrated to yield an expression for the solder volume;

therefore, the volume of the solder results in the following relationship among the geometric parameters, which can be determined as follows

$$\overline{V} = \pi \left\{ \overline{r}_c^2 - \varsigma_0^2 + \varsigma_0 - \frac{1}{3} + \rho_0 \left[ \rho_2 + \varsigma_0 \left( \rho_1 - \rho_2 \right) \right] - \rho_0 \overline{r}_c^2 \left[ \cos^{-1} \left( \frac{1 - \varsigma_0}{\overline{r}_c} \right) - \cos^{-1} \left( - \frac{\varsigma_0}{\overline{r}_c} \right) \right] \right\}$$
(13)

In Eq. (13), the upper and lower bonds of  $\cos^{-1}()$  are limited to 0 and  $\pi$ . During the reflow process, an expression of the vertical reaction force derived on the upper side was

$$F_{r} = \frac{\pi \rho_{2} \lambda h}{2\bar{r}_{c}} \left[ \left( \rho_{1} + \rho_{2} - \sqrt{\frac{4\bar{r}_{c}^{2}}{(\rho_{1} - \rho_{2})^{2} + 1} - 1} \right) \right]$$
 (14)

where  $F_r$  is the reaction force for a single solder ball and  $\lambda$  is the surface tension of the interface between the molten and the atmosphere. accumulation of the package or weight W must balance the total reaction forces of the solder ball or solder bump array. For any arbitrary standoff height, the radius of curvature was determined by iterating the minimum radius of curvature incrementally until the volume of the solder matched the specified volume. Fig. 4 shows the local model of single solder ball with the determined solder profile. The determined solder ball height is 0.374 mm.

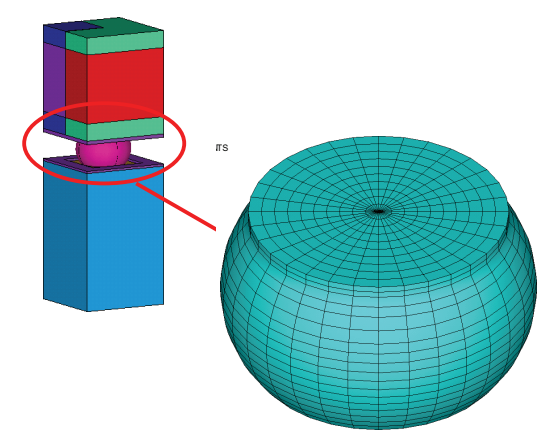


Fig. 4. Local model of single solder ball.

# C. Plastic-Creep Analysis Method

In general, most packaging materials linear elastic considered as temperature-dependent elastic. The solder presents well-known fatigue failure modes attributed to thermal induced strains from CTE mismatch. The strain-induced fatigue can be further divided into two categories, named plastic strain and creep strain. Plastic strain deformation focuses on the time-independent plastic effects, while creep strain accounts for the timedependent effects [24]. Since the plastic and creep properties of the solder are decided, John et al. [25] investigated different methods of implementing thermal cycling analysis, named the dwell creep and full creep methods based on a phenomenological approach to model timedependent plastic and creep deformations. This indicated significant paper differences between the dwell and full analysis results for the solder joint strain responses and the predicted fatigue life. The nature of solder lends itself to creep deformation, which must be accounted for. The solder material must consider as nonlinear with plastic and creep behaviors covering the range of temperatures for thermal cycling (TC) simulation. The solder was assumed to exhibit elastic perfectly plastic behavior after yielding.

# Solder Fatigue Life

Coffin-Manson's law is the most popular fatigue model used to predict the solder fatigue life. Engelmaier [26] proposed a method to correlate the fatigue life obtained at different temperatures and cyclic frequencies with the determination of acceleration factors to predict fatigue behavior in the field from acceleration laboratory tests. The Engelmaier relationship is given by

$$N_f = \frac{1}{2} \left( \frac{\Delta \gamma_{eq}}{2\varepsilon_f'} \right)^{\frac{1}{c}} \tag{15}$$

where  $N_f$  is the number of cycles to failure,  $\Delta \gamma_{eq}$  is the equivalent shear strain range of the solder ball,  $\varepsilon_f'$  is the fatigue ductility coefficient ( $2\varepsilon_f' \cong 0.65$  for eutectic solder). The equivalent shear strain range can be converted from equivalent strain range, that is  $\Delta \gamma_{eq} = \sqrt{3} \times \Delta \varepsilon_{eq}$ , and the value of the variable, c, is a function of frequency and temperature, which is given by

$$C = -0.442 - 6 \times 10^{-4} \times T_{mean} + 1.74 \times 10^{-2} \times \ln(1+f) (16)$$

where  $T_{mean}$  is the mean cyclic solder joint temperature in  $^{\circ}$ C and f is the cyclic frequency in cycles/day.

To consider both creep and plasticity, Hong and Burrell [27] introduced a constitutive theory of isotropic thermoviscoplasticity for modeling the response of thermo-elastic, creep and rate independent plastic deformation. The conventional creep and plasticity concept is used, in which the creep can be described separately from the independent plasticity. Therefore, no interaction between the creep and plasticity will be considered in formulations. In simplified description, the shear strain range,  $\Delta \gamma$ , can be rewritten as

$$\Delta \gamma_{in} = \Delta \gamma_c + \Delta \gamma_p \tag{17}$$

where the  $\Delta \gamma_m$  is the inelastic shear strain range,  $\Delta \gamma_c$  is the creep shear strain range and  $\Delta \gamma_p$  is the plastic shear strain range.

# Validation of Equivalent Global Model

# A. Nonequivalent Global Modeling

In order to verify the equivalent concept, another global model using the actual soldered ball configuration with a course mesh is created in concert with the equivalent soldered bump layer. In this model, the soldered bumps remain as the equivalent layer and are not considered in the actual soldered bump configuration due to there being too many soldered bumps. However, once the simulation results for the soldered balls are satisfied, similar conclusions for the soldered bumps can be deduced. For nonequivalent modeling, a meshing problem exists due to the different pitches of the soldered bumps and balls and around the corners of chips and fillet sites of the underfill. Therefore, the constraint equations between interface face were applied between the middle of the substrate (CEINTF) to avoid the mesh problem. The CEINTF method can be used to tie together two regions with dissimilar mesh patterns by generating constraint equations that connect the selected nodes to the selected elements. It is worth noting that nodes should be selected from the denser mesh region at the bottom surface of the interface, and the elements should be selected from the less-dense mesh region at the upper surface of the interface. Constraint equations are then written that relate the bottom surface and upper surface nodes at the interface. In this analysis, the CEINTF interface was considered in the middle of the substrate. Fig. 5 shows the global nonequivalent finite element model. The creation of a submodel for the soldered ball was the same as equivalent model. At the same time, only one submodel procedure was needed to simulate the stress-strain responses of solder ball.

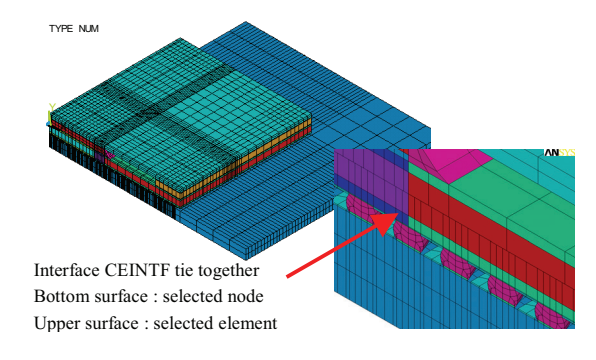
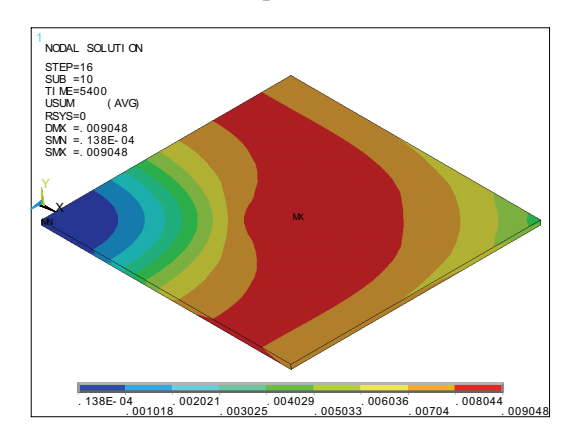


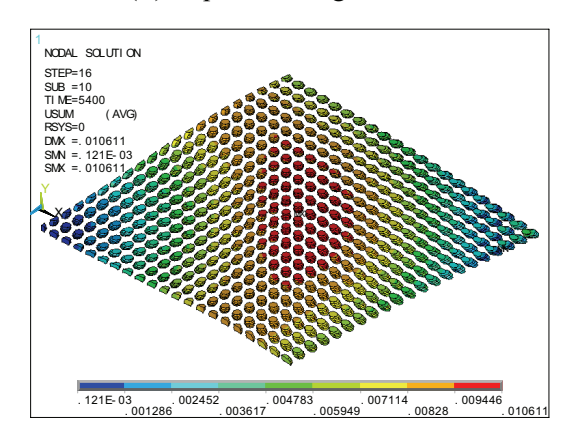
Fig. 5. Nonequivalent global finite element model.

During thermal environment servicing from -40 °C to 125 °C (cph = 2), warping dominated the behavior of the package system. The displacement and strain responses were compared in the final load steps. Fig. 6 shows the total displacement distributions of the solder ball layer between equivalent and nonequivalent global models. The maximum displacement of nonequivalent model was 14.7% higher

than that of equivalent model, and the minimum displacement of nonequivalent model was 88.6% higher than that of equivalent model. The displacement field that equivalent global model provides a higher stiffness for the package minimum displacement system. The exhibited a large difference between equivalent and nonequivalent models for both equivalent soldered layers. However, displacement patterns were quite similar with a relative quality to each of the models, and they did not greatly affect the stress-strain responses.



(a) Equivalent global model



(b) Nonequivalent global modelFig. 6 Total displacement distributions of BGA layer for equivalent and nonequivalent models.

Nevertheless, in view of the range

under the chip, the maximum displacement location occurred just beneath the chip boundary, around the second row. It is worth noting that the failure location of the solder ball under the chip corner was not expected for either model. This might overrule the most serious solder ball location being under the chip corner when 2D finite element analysis was performed by many researchers. Table II shows the fatigue life prediction according to the modified Coffin-Manson model for the solder ball. The life of the solder ball is about 1900 cycles. The predicted lifespans are quite coincident between two models. This shows that the layer equivalent to the soldered balls and bumps is a reliable concept in the finite element analysis of the response of the package during the thermal cycling test.

Table II

Fatigue Life of the Modified Coffin-

Manson Model						
	Max. total	Min. total	Total shear	Life		
	shear	shear	strain	(cycles)		
	strain	strain	range			
Equivalent global model	0.08262	0.05854	0.02408	1886		
Nonequivalent global model	0.06876	0.04469	0.02407	1892		

## B. Shadow Moiré Measurement

Furthermore, the vertical deformations of equivalent global model were solved by defining specific temperature differences and used to compare with measurement results for model validation purposes. The reference temperature is 25 °C and the verification temperatures are at 75 °C and 125 °C to experience both heating and cooling periods. An AkroMetrix TM

TherMoiré system PS200 model was used to measure the package warpage. The absolute deformation fringe patterns on the substrate side were caught at temperatures processed with installed analysis software to determine the relative deformation profiles along the diagonals. Table III lists the comparison results of the warpage. An average of 6.54% difference exists at 75°C and 0.42% difference exists at 125°C between the simulation and measurement results. The finite element model is qualified to conduct reliability studying.

TABLE III
Comparison of Warpage Results

Temp.	Sh	adow Mo	Simulation	Error	
	Heating	Cooling	Average	Simulation	(%)
75℃	46 μm	28 μm	37 μm	34.58 μm	6.54
125℃	72 μm	_	72 μm	71.70 μm	0.42

### **Board-level reliability studying**

Thermal cycling test is a common method to evaluate the package-level and board-level reliabilities. This test was conducted to determine the ability of solder interconnects to withstand thermomechanical stresses induced by alternative high and low temperature extremes. Testing J condition is usually adopted for FCBGA package board-level reliability based on JESD22-A104-B. Fig. 7 shows the temperature cycles where the ramp up/down rate is 10°C/min, the dwell time at each extreme temperature is 10 min and is 40 min/cycle. Three frequency temperature cycles are considered for the simulation resulting from strain envelope saturation assumption.

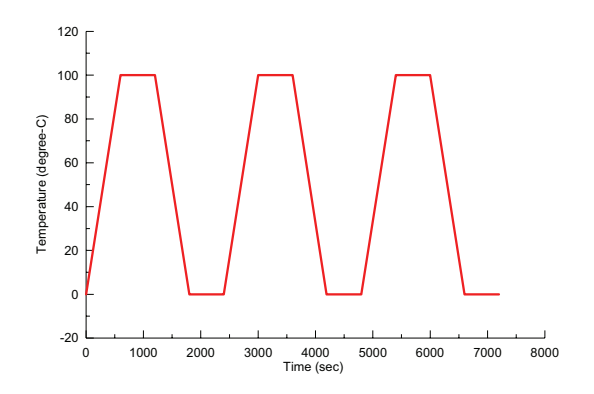


Fig. 7. Temperature cycle for board-level reliability evaluation  $(0^{\circ}C/100^{\circ}C, \text{cph} = 1.5)$ 

Fig. 8 shows the equivalent strain contour on the BGA layer. The simulation result shows identical to the actual failure locations, which are beneath the die area. Fig. 9 shows the equivalent strain contour of the local solder ball model after three temperature cycles. The maximum strain occurs at the package side and this symptom is also exactly identical to the cross-section and SEM inspections.

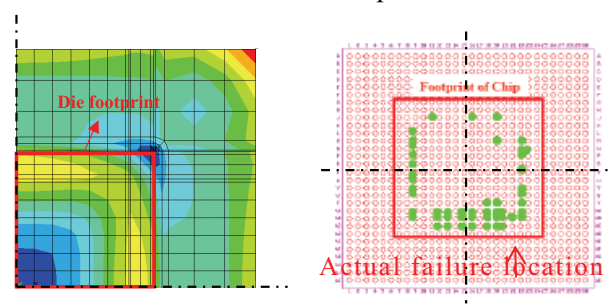


Fig. 8. Equivalent plastic strain contour on BGA layer and actual failure locations.

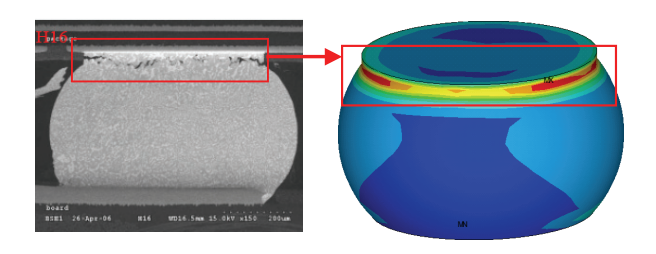


Fig. 9. Equivalent strain contour of critical solder ball and a SEM inspection photo.

#### Conclusion

This paper introduced 3-D equivalent global model with a local submodel technique to address critical failure locations. Full model feasibility, computation time saving and symptom correlation were the major contributions. The number cycles to failure in solder ball life was predicted based on the Coffin-Manson fatigue model. A HFCBGA package case is studied with the provided experimental data. According to the prediction fatigue life result, the determined solder ball life shows with satisfactory agreement the characterization life of experimental data.

## References

- [1] J. H. Lau, "Ball Grid Array Technology," New York: McGraw -Hill, (1955)
- [2] B. M. Romenesko, "Ball Grid Array and Flip Chip Technologies: Their Histories and Prospects," The International Journal of Microcircuits and Electronic Packaging, Vol. 19, No. 1, pp. 64-74, (1996)
- [3] K. Doi, "Prediction of Thermal Fatigue Life for Encapsulated Flip Chip Interconnection," The International Journal of Microcircuits and Electronic Packaging, Vol. 19, No. 3, pp. 231-236, (1996)
- [4] H. L. Pang, T. I. Tan, K. S. Suresh, "Thermal - Mechanical Analysis of Solder Joint Fatigue and Creep in a Flip Chip on Board Package Subjected to Temperature Cycling Loading," Electronic Components and Technology Conference, pp. 878-883, (1998)

- [5] H. Reichl, A. Schubert, M. Töopper,
   "Reliability of Flip Chip and Chip Size Packages," Microelectronics
   Reliability, Vol. 40, pp. 1243-1254,
   (2000)
- [6] K. N. Chiang, Z. H. Liu, C. T. Peng, "Parametric Reliability Analysis of No-Underfill Flip Chip Package," IEEE Trans Compon Packag, Vol. 24, No. 4, pp. 635-640, (2001)
- [7] J. Wang, Z. Qian, D. Zou, S. Liu, "Creep Behavior of a Flip-Chip Package by Both FEM Modeling and Real Time Moiré Interferometry," ASME J of Electron Packag, Vol. 120, pp. 179-84, (1998)
- [8] Q. Zhang, A. Dasgupta, D. Nelson, H. Pallavicini, "Systematic Study on Thermal-Mechanical Durability of Pb-Free Assemblies: Experiments and FE Analysis," ASME J of Electron Packag, Vol. 127, pp. 415-428, (2005)
- [9] S. Cho, B. Han, J. Joo, "Temperature Dependent Deformation Analysis of Ceramic Ball Grid Array Package Assembly Under Accelerated Thermal Cycling Condition," ASME J of Electron Packag, Vol. 126, pp. 41-47, (2004)
- [10] W. W. Lee, L. T. Nguyen and G. S. Selvaduray, "Solder joint fatigue models: review and applicability to chip scale packages", Microelectronics Reliability, Vol. 40, pp. 231-244, (2000)
- [11] G. Gustaffon, I. Guven, V. Kradinov and E. Madenci, "Finite Element Modeling of BGA Packages for Life Prediction", Electronic Components and Technology Conference, pp. 1059-1063, (2000)

- [12] V. Sarihan, "Energy Based Methodology for Damage and Life Prediction of Solder joints under Thermal Cycling", IEEE, pp. 32-38, (1993)
- [13] J. H. Lau, "Effects of Built-Up Circuit Board Thickness on the Solder Joint Reliability of a Wafer Level Chip Scale Package (WLCSP)", Int' 1 Symp on Electronic Materials and Packaging, pp. 115-126, (2000)
- [14] B. Z. Hong and L. S. Su, "On Thermal Stresses and Reliability of a PBGA Chip Scale Package", Electronic Components and Technology Conference, pp.503-510, (1998)
- [15] B. A. Zahn, "Impact of Ball Via Configurations on Solder Joint Reliability in Tape-Based, Chip-Scale Packages", Electronic Components and Technology Conference, pp.1475-1483, (2002)
- [16] B. Z. Hong, "Finite Element Modeling of Thermal Fatigue and Damage of Solder joint in a Ceramic Ball Grid Array Package", Journal of Electronic Materials, Vol. 26, No. 7, pp. 814-820, (1997)
- [17] B. Vandevelde, M. Gonzalez, E. Beyne, G. Q. Zhang and J. Caers, "Optimal Choice of FEM Damage Volumes for Estimation of the Solder Joint Reliability for Electronic Package Assemblies", Electronic Components and Technology Conference, pp.589-596, (2003)
- [18] I. Guven, V. Kradinov, E. Madenci and J. L. Tor, "Solder Joint Life Prediction Model Based on the Strain Energy Density Criterion",

- Electronic Components and Technology Conference, pp.214-220, (2003)
- [19] J. H. L. Pang, C. W. Seetoh and Z. P. Wang, "CBGA solder joint reliability evaluation based on elastic plastic creep analysis", ASME J of Electron Packag, Vol. 122, No. 3, pp. 255-261, (2000)
- [20] B. A. Zahn, "Solder Joint Fatigue Life Model Methodology for 63Sn/37Pb and 95Sn4Ag0.5Cu Materials", Electronic Components and Technology Conference, pp. 83-94, (2003)
- [21] R. M. Jones, Mechanics of Composite Materials, McGraw-Hill, (1975)
- [22] Y. Yuan, "Computational Material Property Simulation for Laminated Composites", IEEE, pp. 869-875, (2006)
- [23] S. M. Heinrich, M. Schaefer, S. A. Schroeder and P. S. Lee, "Prediction of Solder Joint Geometries in Array-Type Interconnects", ASME J of Electron Packag, Vol. 118, pp. 118-121, (1996)
- [24] P. M. Hall, Creep and Stress Relaxation in Solder Joints (Chapter 10), J.H. Lau, editor, Solder Joint Reliability Theory and Application, New York, Van Nostrand Reinhold, (1991)
- [25] J. H. L. Pang, D. Y. R. Chang and T. H. Low, "Thermal Cycling analysis of Flip-Chip Solder Joint Reliability", IEEE Transaction on Components and Packaging Technology, Vol. 24, No. 4, pp. 705-712, (2001)
- [26] W. Engelmaier, "Fatigue Life of

- Leadless Chip Carrier Solder Joints During Power Cycling," IEEE Trans Components and Manufacturing Technology, Vol. 6, No. 3, pp. 52-57, (1983)
- [27] B. Z. Hong and L. G. Burrell,
  "Nonlinear Finite Element
  Simulation of Thermo-viscoplastic
  Deformation of C4 Solder joints in
  High Density Packaging Under
  Thermal Cycling", in Intersociety
  Conference on Thermal Phenomena,
  pp.117-125, (1994)
- [28] R. G. Ross, L. C. Wen, G. R. Mon and E. Jetter, "SolderCreep-Fatigue Interactions with Flexible Leaded Parts", ASME J of Electron Packag, Vol. 114, pp. 185-192, (1992)